Available online at www.sciencedirect.com
SCIENCE DIRECT
ELSEVIER
Polymer 46 (2005) 6522–6530
polymer
www.elsevier.com/locate/polymer

Application of an interpenetrating network model to the solid deformation of a quenched isotactic polypropylene film☆

Yihu Song[a,*], Norio Nemoto[b]

[a]Institute of Polymer composite, Department of Polymer Science and Engineering, Zhejiang University, Hangzhou 310027, China
[b]Department of Molecular and Material Sciences, IGSES, Kyushu University, Hakozaki, Fukuoka 812-8581, Japan

Received 15 October 2004; received in revised form 5 April 2005; accepted 12 May 2005

Abstract

The molecular orientation and deformation mechanisms of a quenched isotactic polypropylene (iPP) film deformed at temperatures between 303 K and the melting point are studied. At draw temperature T_E less than 400 K where the degree of crystallinity does not change markedly, a linear relationship between molecular orientations of the crystalline and the amorphous phases is revealed and the slope is estimated about 1.82. The interpenetrating network (IPN) model, that takes into account the plastic response of the crystalline (C) network formed by a small portion of crystallites adhered through intercrystalline links and the pseudo-affine deformation of the crystallite enhanced amorphous matrix (CEAM) network, is able to account for inhomogeneous deformation behavior on the mesoscale accompanied with the localized necking in this T_E range. Meanwhile, the initial Young's modulus and the true yield stress exerted by the deformation of the rigid C network exhibit the Arrhenius type of dependence on T_E. The apparent shear modulus of the CEAM network as a function of T_E is discussed in relation to variations in numbers and average molecular weights of the crystalline and the amorphous sequences being manifested by small consecutive endothermic and exothermic peaks in the DSC curve. The IPN model becomes invalid for deformations above $T_E = 400$ K where morphological changes are induced due to melting of crystallites as proved from the DSC measurement.

Keywords: Polypropylene; Deformation; Interpenetrating network model

1. Introduction

Using an equipment for simultaneous kinetic measurements of microscopic infrared (MicIR) dichroism from a predetermined mesoscale sampling area and of macroscopic stress of a polymer thin film subjected to uniaxial stretching at a constant elongation rate [1], we have studied the molecular orientation of a quenched isotactic polypropylene (iPP) film during the necking at 303 K [2]. The deformation is truly inhomogeneous on a macroscopic scale. However, drastic deformation and molecular orientation mainly occur in the neck shoulder [3]. We disclosed a pseudo-affine deformation for the amorphous phase up to a local extension ratio $\lambda_{Meso} \sim 4.5$ based on the relationship between the orientation function of the amorphous phase, f_{am}, and λ_{Meso} in situ determined on a mesoscale of 200 μm. Since the orientation function of the crystalline phase, f_c, has been found to be in proportion to f_{am} in the same λ_{Meso} region [3], the average orientation function, f_{av}, as a function of λ_{Meso} can also be described by the affine model.

By measuring the molecular orientation along the draw axis of a quenched film stretched to different macroscopic strains, we showed that the pseudo-affine deformation is applicable up to a limiting value of $f_{am} \approx 0.45$ for fully stretched strands, which should be recognized as a key value to stipulate an upper limit of the pseudo-affine type of deformation occurring in the narrow neck shoulder region [4]. This value is located near the boundary between the neck shoulder and the neck entity, which partly explains why the neck shoulder appears to smoothly propagate.

We proposed an interpenetrating network (IPN) model for interpreting the true stress–strain relationship of a mesoscale area suffering from the necking in the quenched

☆Part V of deformation mechanisms of polymer thin films by simultaneous kinetic measurements of microscopic infrared dichroism and macroscopic stress.

* Corresponding author. Tel.: +86 571 87953075; fax: +86 571 87951635.
E-mail address: s_yh0411@zju.edu.cn (Y. Song).

0032-3861/$ - see front matter © 2005 Elsevier Ltd. All rights reserved.
doi:10.1016/j.polymer.2005.05.058

iPP film [4]. In this model, a small portion of crystallites adhered through intercrystalline links [5] forms a rigid crystal (C) network that penetrates through a soft crystallite enhanced amorphous matrix (CEAM) network. The deformation of the C network during the necking is described using Takayanagi tie molecule model [6], while the deformation of the CEAM network should obey the affine deformation model as far as the elongation temperature (T_E) is above the glass transition temperature (T_g) of the amorphous phase [4]. After tie molecules are pulled out, the intercrystalline links flow and exert viscous force in the neck shoulder region. Since the number density of intercrystalline links does not change as far as volume constancy is kept during stretching, the true stress supported by the C network remains constant after yielding, but that from the CEAM network increases by stretching. This model with slight alternation is also validated in films of poly(ether-*block*-amide) copolymers as well as films of a metallocene polypropylene, an ethylene–butylene rubber and their 80 wt/20 wt blend at room temperature [7].

The IPN model might be comparable with the previous molecular network concept. Elastically effective network strands in amorphous regions have their ends more or less fixed either by entangling or by anchoring in the adjacent crystallites so as to set up a network underpinning the semicrystalline morphology, which is of key importance in determining the drawing process [8]. Shrinkage and shape memory effects in the deformed materials strongly support the presence of a molecular network [9]. Although stretching of semicrystalline polymer specimens induces plastic deformations in the crystalline phase, the amorphous phase at $T_E \gg T_g$ should behave elastically whenever the semicrystalline structure is considerably stable during the deformation. Neutron scattering experiments have been performed to determine the radius of gyration in polyethylene fibers drawn beyond the necking and the stress-softening regions. The results show that, at T_Es between 343 and 363 K depending on the molecular weight, there is no evidence for any local melting and molecules appear to deform affinely through the necking, whereas drawing at higher T_Es leads to local melting and the affine model does not hold anymore [10]. It seems that, below the melting point T_m, there exists an upper limiting temperature above which the affine deformation of amorphous chains in semicrystalline polymers cannot be realized. An issue arises where this limiting temperature is located for the quenched iPP film with the smectic crystalline structure.

Relative contributions from the crystalline and the amorphous phases to the true stress–strain relationship should alter with variations in deformation temperature. The cooperativity of the two phases, or the two networks in the proposed model, remains ambiguous in our previous paper [4]. Since the cooperativity might be a function of temperature, we shall in this study further examine the applicability of the this model to the plastic deformation of the quenched iPP film drawn in a relatively broad temperature region above room temperature yet below T_m. The influence of T_E will be discussed on the basis of molecular orientation combing with the true stress–strain relationship. Especially, discussions will be made to key parameters governing the deformations of the C and the CEAM networks as a function of T_E.

2. Experimental section

2.1. Materials and sample preparation

iPP pellets with $M_W = 3.7 \times 10^5$ g mol^{-1} were compressed at 483 K for 5 min to form a film with an average thickness of ca. 30 μm, which was then quenched into an ice water.

2.2. Apparatus and method

The setup detail of the equipment, the kinetic measurement of MicIR dichroism and the data analysis procedure are described in the earlier papers [1,2]. This equipment offers a kinetic measurement of $AC(t) = A_{\parallel}(t) - A_{\perp}(t)$ and $DC(t) = A_{\parallel}(t) + A_{\perp}(t)$ alternately at a time interval of 30 s. Here $A_{\parallel}(t)$ and $A_{\perp}(t)$ are the polarized spectra at stretching time t with the IR radiation parallel and perpendicular to the draw axis, respectively.

The film samples with an initial length $L_0 = 2$ mm and an initial width $W_0 = 3$ mm were fastened between the two clamps and were stretched at a constant elongation rate of 0.05 min^{-1} with simultaneous movement of the clamps to the opposite directions.

The viewing field for sampling the MicIR dichroism was 200×200 μm^2. An insulating protector with a potassium bromide window was used to cover the sample cell for controlling the temperature as well as protecting the objective of the IR microscope. The MicIR dichroism was sampled from the film center. Stretching was started 1 min after the desired elongation temperature T_E was attained. We measured the film width and thickness in the film center so as to derive the local draw ratio λ_{Meso} and the true stress σ utilizing that the specific volume is kept constant during uniaxial stretching [3].

From the dichroism of a desired absorbance band, the orientation function

$$f = \frac{3\langle \cos^2\theta \rangle - 1}{2} \tag{1}$$

can be derived from

$$f = \frac{2A(t)}{3 - A(t)} \frac{R_0 + 2}{R_0 - 1} \tag{2a}$$

with

$$A(t) = \frac{AC(t)}{DC(t)} \tag{2b}$$

Here, θ is the orientation angle of a chain segment making with the draw-axis, and $R_0 = 2\cot^2\psi$ is the perfect dichroic ratio of a transition moment making an angle ψ with the direction of the molecular main chain axis. The 973 cm^{-1} π-band belongs to the CH_3 rocking and the axial and equatorial C–C stretching modes in both the amorphous and the crystalline phases [11], whose dichroism allowed us to derive the orientation function f_{av} in relation to the average chain orientation under the viewing field [12,13]. The f_c was determined from the π-band at 998 cm^{-1} involving the CH_3 rocking, the C–CH_3 stretching, the CH bending and the CH_2 twisting modes in the crystalline phase [12,13].

Thermal behaviors of the quenched film was examined from differential scanning calorimetry (DSC) analysis using a DSC-8240B calorimeter with a TAS-100 controller (Rigaku) at a heating rate of 2 °C min^{-1} under dry nitrogen atmosphere. The starting temperature in DSC measurement was 300 K. The temperature of the calorimeter was calibrated from the observed melting points of ultra-pure indium and short *n*-alkanes. The first run data were analyzed. The fractional crystallinity V_c as a function of temperature was estimated according to the First Law method [14].

3. Results

3.1. Nominal stress and molecular orientation at various T_Es

Fig. 1(a) shows the nominal stress σ_n in a range of T_E from 303 to 430 K against stretching time t in proportion to nominal strain ε_n. Decrease in σ_n with increasing T_E directly reflects the reduction in the intermolecular force. The yielding time where σ_n reaches the maximum or plateau is prolonged and the load drop for the strain-softening in convention is lowered as T_E is increased up to 399 K. The yield strain decreases slightly and the strain-softening disappears for 413 K $\leq T_E \leq$ 430 K. When T_E is increased in the narrow range from 413 to 421 K, the stress level is slightly improved probably due to the thermal recrystallization accelerated by stretching.

The f_{av} profiles selectively shown in Fig. 1(b) reveal that the necking is crucial for the local deformation in the T_E range of 303–399 K where the neck propagation through the viewing field causes the rapid molecular orientation [2,3]. The following slow orientation is attributed to the further deformation in the necked region namely the neck entity. The molecular orientation is, irrespectively of T_E, closely related to the initial position of neck initiation and the subsequent necking propagation. During the deformation at $T_E \geq 413$ K, f_{av} takes a wavy profile against time in spite of the overall increment. This result suggests that the original film center might be continuously moved back and forth during deformation, which resulted in the MicIR dichroism data actually sampled from different areas in the film.

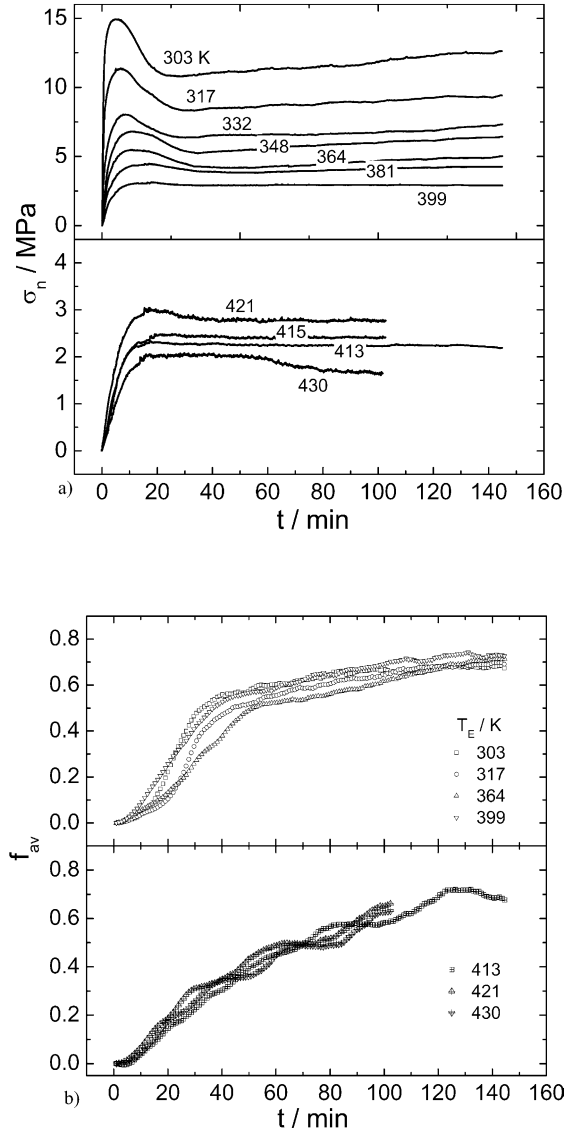

Fig. 1. Nominal stress σ (a) and orientation function f_{av} (b) as a function of stretching time t for the quenched film draw at various T_Es.

3.2. Thermal behaviors

The smectic phase in quenched iPP film might be transformed to α-form crystal at high temperatures or/and under uniaxial loadings, whereas deformation also produces the smectic phase by pulling-out helical chains from lamellae of the α-form [15–17]. Fig. 2 shows the DSC curve and the resulting V_c as a function of temperature. As found by Wang [18] et al. and also by Androsch and Wunderlich [19], a small endotherm centered at 327 K, a small exotherm centered at 368 K and a sharp endotherm peak centered at 438 K are seen for the quenched iPP film with a smectic crystalline form. These three events are related to the melting process of the smectic form, the

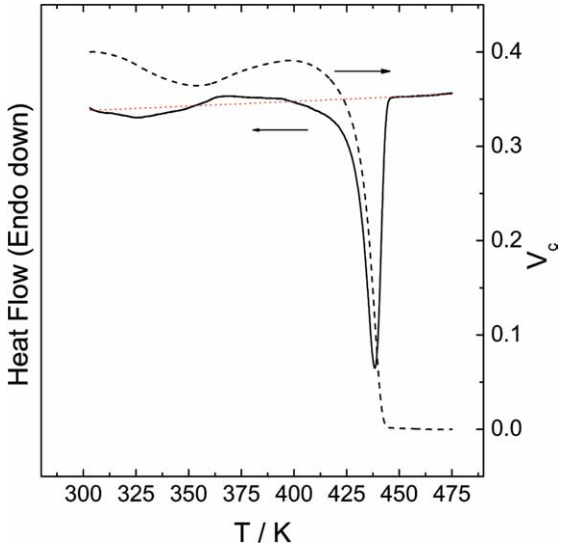

Fig. 2. DSC curve of the quenched iPP sample subjected to heating under a rate of 2 °C min^{-1} and the degree of crystallinity as a function of temperature.

recrystallization process to form the α-monoclinic phase, and the final melting of the α crystals, respectively, which are well visualized in the temperature dependence of V_c.

3.3. Relationship between f_c and f_{am}

The relationship between f_c and f_{av} is presented in Fig. 3(a) in which f_c is vertically shifted for help of view. During the deformation, the neck may move continuously. The data are really sampled from different areas, resulting in slight fluctuations. We could distinguish presence of a linear portion in the f_c–f_{av} relation for $f_{av} \leq 0.5$, approximately. Plotting the slope K' of the linear portion as a function of T_E in Fig. 3(b), we find a transition at 400 K below which the proportional constant $K' \approx 1.39$ is likely independent of T_E. K' appears to increase abruptly above the transition temperature in the partially melted samples.

We already showed that a linear relationship of $f_c = Kf_{am}$ holds during the pseudo-affine deformation of the quenched film at 303 K [3]. On the basis of the two-phase model [9],

$$f_{av} = V_c f_c + (1 - V_c) f_{am} \quad (3)$$

the proportional constant K can be estimated from K' and V_c,

$$K = \frac{(1 - V_c)K'}{1 - V_c K'} \quad (4)$$

and is plotted against T_E in Fig. 3(b). Although there is a slight change in V_c at temperatures below 400 K, $K \approx 1.82$ is almost independent of T_E and is very close to the previous value of $K = 1.85$ [3]. The constant K value in this T_E region suggests that the molecular orientation of crystallites is only a function of the deformation of amorphous chains during the necking, and is independent of deformational stress and the possible smectic-to-monoclinic transformation [20].

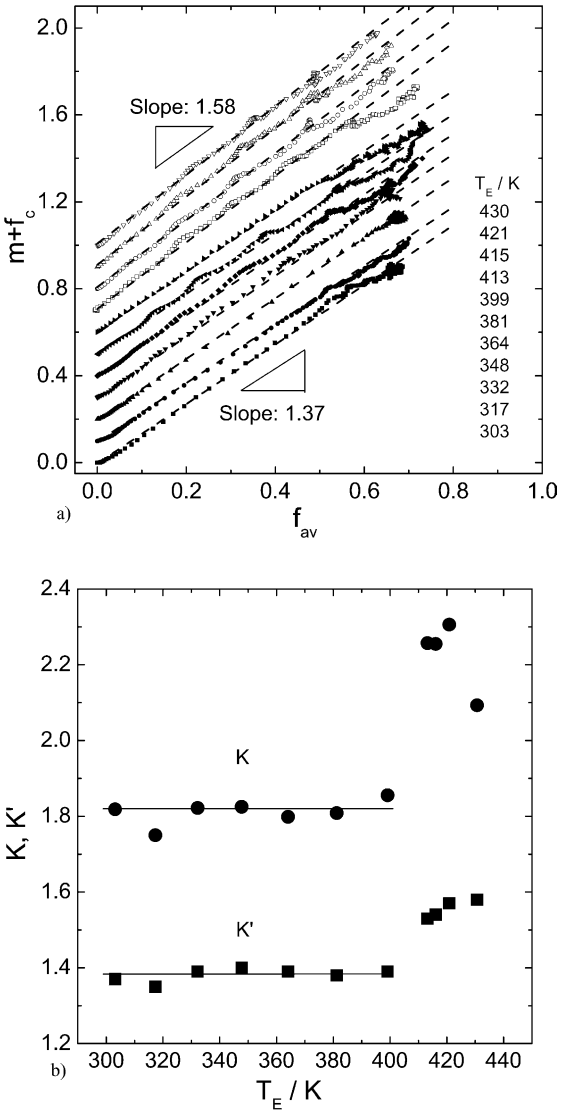

Fig. 3. (a) Relationship between f_c and f_{av} for the deformation at various T_Es from the top at $T_E = 430$ K to the bottom at $T_E = 303$ K and (b) T_E dependences of proportional constants K' and K for the linear portions of the f_c–f_{av} and the f_c–f_{am} relationships.

Though heating weakens the intermolecular interaction and gives chains energy for uncoiling and also for slipping past each other even under small stresses, the crystallites are still strong enough in comparison with the amorphous phase. Therefore, according to the Takayanagi tie molecule model [6], pulling-out of tie molecules from crystalline lamellae is the main process that gives rise to the localized necking and facilitates the crystalline orientation matching to that of the amorphous phase. At higher T_Es located in the main melting region of the α crystals, the abrupt increase in K is mainly attributed to the decrease of V_c and the strain-induced recrystallization.

3.4. Applicability of the IPN model

From time profiles of σ_n and f_{av} as well as the linear

relationship between f_c and f_{am}, it seems reasonable to consider that the mesoscale necking at 303 K$\leq T_E \leq$399 K should obeys the same pseudo-affine deformation mechanism with constant volume. Then it may be worthwhile to examine applicability of the IPN model [4] to the true stress–strain behaviors at this T_E range. This model simply assumes that the total true stress σ is given as the sum of the true stresses, σ_C and σ_{CEAM}, supported by the C and the CEAM networks, respectively, as

$$\sigma = \sigma_C + \sigma_{CEAM} \tag{5a}$$

$$\sigma_C = \sigma_y(C) \tag{5b}$$

$$\sigma_{CEAM} = M_{PT}(\lambda_{Meso}^2 - \lambda_{Meso}^{-1}) \tag{5c}$$

Here $\sigma_y(C)$ is the true yielding stress of the C network and M_{PT} is the apparent shear modulus of the CEAM network. In this model, the true yield stress σ_y is given as a sum of $\sigma_y(C)$ and the stress $\sigma_{CEAM}(\varepsilon_y) = M_{PT}(\lambda_y^2 - \lambda_y^{-1})$ supported by the CEAM network at the yielding point. In the previous study, we supposed that σ_y can be put equal to $\sigma_y(C)$ during the necking at such a low temperature of $T_E =$ 303 K that $\sigma_{CEAM}(\varepsilon_y)$ may be considered much smaller than σ_y [4]. This becomes questionable at elevated T_Es where the total stress from the film is reduced considerably. Therefore, we in this work treat $\sigma_y(C)$ and M_{PT} as two adjustable parameters for performing data fitting to the measured data and consequently for an estimate of the yield strain $\varepsilon_y = \lambda_y - 1$.

Fig. 4 shows the true stress–strain (σ–λ_{Meso}) relationship together with the curves calculated on the basis of Eqs. (5a)–(5c) for $\sigma \geq \sigma_y$. It is seen that the IPN model fairly describes the mesoscale deformation of necking at 303 K$\leq T_E \leq$399 K. This suggests that our model is undoubtedly applicable so long as the deformation dominantly occurs in such localized area as the neck shoulder where molecules are deformed at a constant strain rate up to large strains giving a constant σ_c.

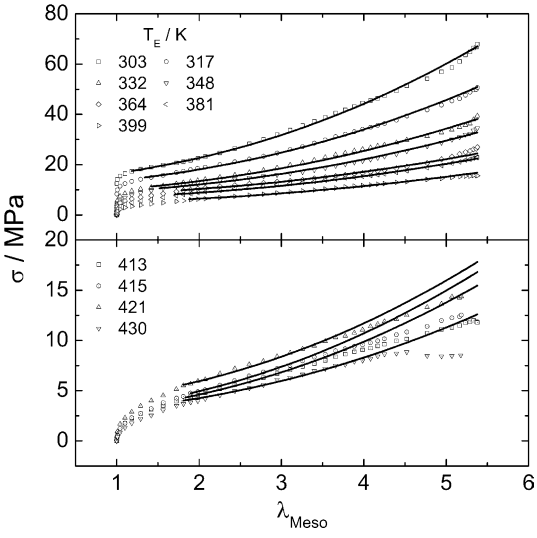

Fig. 4. True stress–strain relationship for the quenched film at 303 K$\leq T_E \leq$430 K. The curves are calculated according to Eqs. (5a)–(5c).

In the T_E region of 413–430 K, this model can not account for the deformation though a qualitative agreement is achieved at a middle strain range of $\lambda_{Meso} \approx$ 2.0–3.5. The measured σ is located below the predicted one at high strains, which is partially attributed to the breakdown of crystals and the local melting dominating over the thermal recrystallization as well as the molecular orientation.

4. Discussion

The aforementioned results disclose three characteristics for the deformation at 303 K$\leq T_E \leq$399 K: (1) the necking dominates the local deformation and the molecular orientation, (2) the slopes K' and K remain constant, (3) the IPN model can be successfully applied to the σ–λ_{Meso} relationship. In the following sections, we focus on the behaviors of the C and the CEAM networks at this T_E range. The molecular orientation and the local deformation show completely different behaviors in a narrow T_E range 413–430 K located in the main melting region on the DSC curve. Invalidation of the IPN model shall be discussed qualitatively in brief.

4.1. Young's modulus and yielding of the film

The solid symbols in Fig. 5 shows the Young's modulus E of the film as determined from the initial slope of the σ–λ_{Meso} curve, the true yield stress σ_y and the reciprocal of the yield strain ε_y^{-1} against the reciprocal of T_E. Dependences of E, σ_y, and ε_y^{-1} on T_E^{-1} are found to follow the Arrhenius law at 303 K$\leq T_E \leq$399 K regardless of variations in V_c and lamellar thickness [21]. The apparent activation energies are estimated 35.7$\pm$0.9, 11.7$\pm$0.5, and 12.9$\pm$0.6 kJ mol^{-1} to E, σ_y, and ε_y^{-1}, respectively. Finite integral of σ from zero to ε_y, i.e., $U_y = \int_0^{\varepsilon_y} \sigma d\varepsilon$ with $\varepsilon = \lambda_{Meso} - 1$, gives yield energy. As shown by the solid symbols in Fig. 6, the U_y value seems independent of T_E up to 400 K and roughly takes a constant value of 3.5$\pm$0.1 MJ m^{-3}.

Above T_E=413 K the Arrhenius law does not hold anymore. The film yields at $\varepsilon_y \approx$ 0.8–0.9 and E is smaller than the values predicted by the Arrhenius law. The deviation from the simple Arrhenius type of temperature dependence is also reflected in U_y that shows an abrupt reduction above 400 K as T_E approaches the melting point. The deviation is consistent with the onset of melting at 398 K in the DSC curve.

Nitta and Takayanagi [22] have proposed a lamellar-cluster model, which assumes that tie molecules between adjacent lamellar clusters produce concentrated load acting on the cluster surface, leading to the bending deformation of the clusters. When the strain energy stored by the bending deformation reaches a critical value, the clusters disintegrate and the sample yields. The model predicts that ε_y is

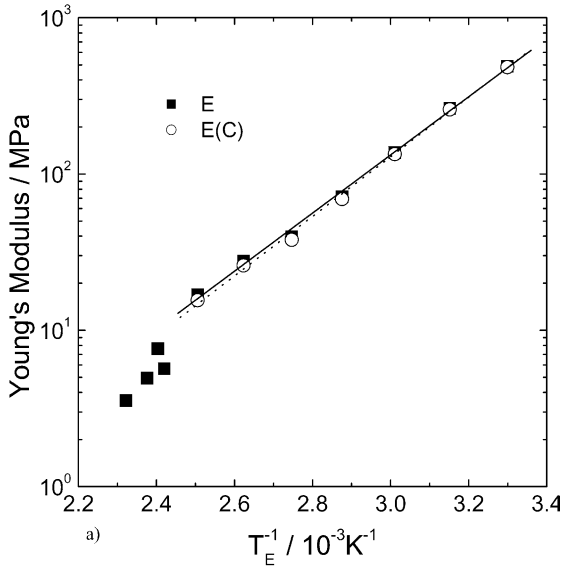

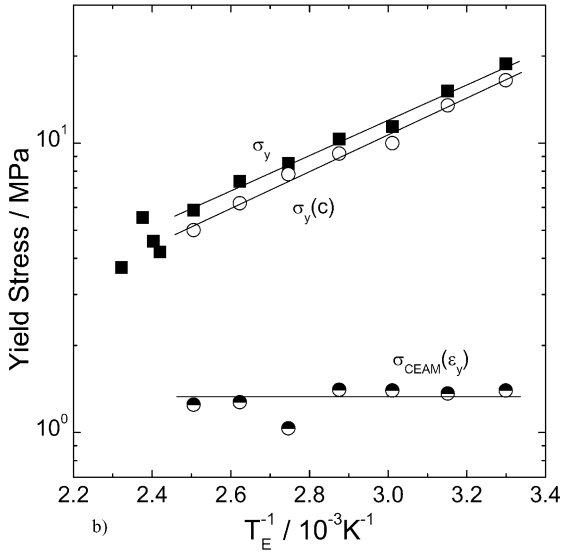

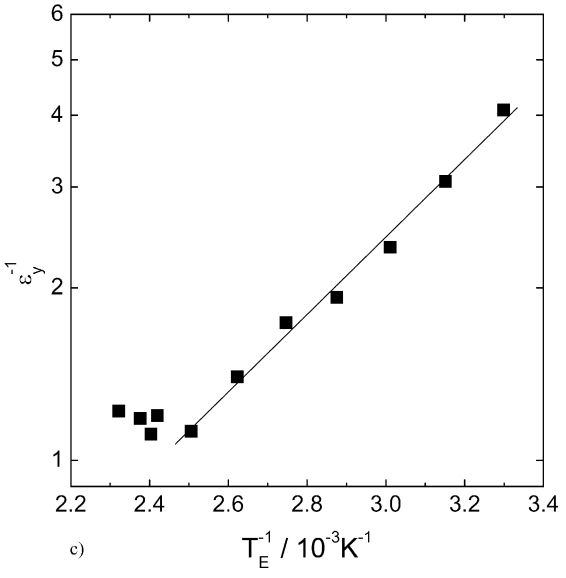

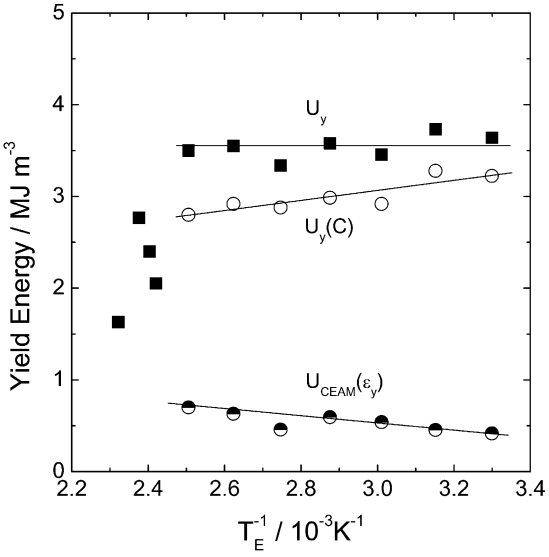

Fig. 6. Yielding energy U_y and $U_y(C)$ for the film and the C network respectively as a function of reciprocal of T_E. U_y is determined from the true stress–strain relationship of the film and $U_y(C)$ is calculated according to $U_y - U_{CEAM}(\varepsilon_y)$. The strain energy of the CEAM network stretched up to the yielding point, $\sigma_{CEAM}(\varepsilon_y)$, is also shown. The lines are drawn for guide of eyes.

inversely proportional to σ_y under constant U_y, which was confirmed in a binary blend of iPP/rubbery ethylene-1-hexene copolymer stretched at room temperature with a crosshead speed of 5 mm min^{-1}. Plotting σ_y against ε_y^{-1} in Fig. 7, we found that the linear relationship holds at 303 K $\leq T_E \leq$ 399 K. The slope 4.85 ± 0.1 is in fair agreement with the value of $\sim$5.2 estimated from Fig. 3 in Ref. [22]. It is suggested that the yielding is exclusively determined by the crystalline phase via the same underlying mechanism. This is reasonable only when the crystals are strong enough in comparison with the amorphous chains and there is no local melting induced by the strain-energy.

4.2. Deformation of the C network

The Young's modulus $E(C)$ of the C network is estimated from $E(C) = E - 3M_{PT}$. The Arrhenius plots of $E(C)$ and $\sigma_y(C)$ are represented as hollow symbols in Fig. 5(a) and (b), respectively. At 303 K $\leq T_E \leq$ 399 K, the apparent activation energies are estimated 36.3 ± 0.9, and 12.1 ± 0.6 kJ mol^{-1} to $E(C)$ and $\sigma_y(C)$, being very slightly higher than those from E and σ_y, respectively. This result implies that the initial deformation and the yielding are controlled by two respective activation mechanisms in the C network.

Fig. 5. (a) Young's modulus E and $E(C)$ for the film and the C network respectively as a function of reciprocal of T_E, (b) true yield stress σ_y and $\sigma_y(C)$ for the film and the C network respectively as a function of reciprocal of T_E, and (c) reciprocal of yield strain ε_y^{-1} as a function of reciprocal of T_E. The solid lines are drawn according to the Arrhenius law. The true stress at the yield strain, $\sigma_{CEAM}(\varepsilon_y)$, supported by the CEAM network is also shown in (b), which discloses that it is independent of T_E.

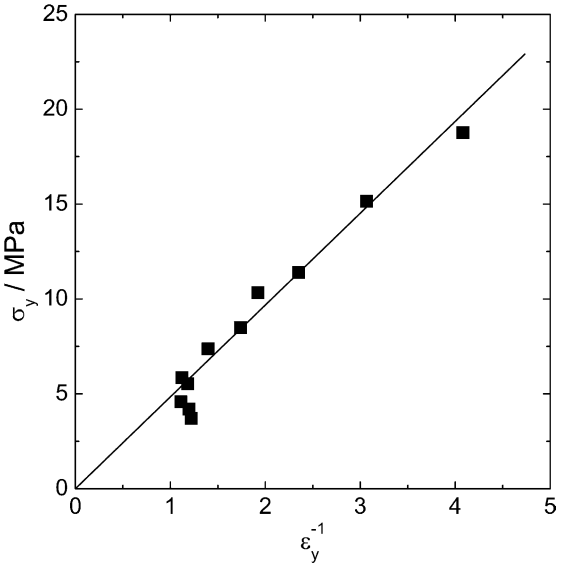

Fig. 7. Relationship between true yield stress σ_y and reciprocal yield strain ε_y^{-1} for the film.

The rigid C network is composed of almost pure crystallites firmly adhered through inextensible intercrystalline links which concentrate applied stress and induce lamellae to yield in a position close to their attachment points. Deformation in the neck shoulder region induces irreversible structural changes in the C network and the force exerted by individual intercrystalline links undergoing the plastic flow is the viscous force depending on T_E. Because the contribution of the CEAM network to stress below the yielding point is considerably small, E and σ_y from the bulk deformation appear to follow the Arrhenius laws.

The IPN model can be regarded as the parallel arrangement of the C and CEAM elements adhered to the lamellar wall, which guarantees the application of Eqs. (5a)–(5c). The yield energy is thereby comprised of two different types of energies, one being the storage one related to deformation of the CEAM network and the other the dissipative energy to be used up for pulling out of chains adhered to the intercrystalline links from lamellae. Only the latter facilitates to liberate energy accumulated in deformed lamellae. In spite of the lack of a theoretical formulation for the σ–λ_{Meso} relationship of the C network below the yielding point, its yield energy, U_y(C), may be estimated from $U_y - U_{CEAM}(\varepsilon_y)$, where $U_{CEAM}(\varepsilon_y) = \int_0^{\varepsilon_y} \sigma_{CEAM} d\varepsilon$ represents the strain energy of the CEAM network stretched up to the yielding point. As shown in Fig. 6, U_y(C) decreases and $U_{CEAM}(\varepsilon_y)$ increases slightly with increasing T_E from 303 to 399 K. On the other hand, Fig. 5(b) reveals that $\sigma_{CEAM}(\varepsilon_y) \approx 1.3$ MPa seems independent of T_E, which is also a crucial factor for the yielding of the C network.

The treatment of Nitta and Takayanagi [22] did not distinguish contributions of the crystalline and the amorphous phases. Our data suggest that constant U_y(C) is not satisfied (Fig. 6) for the yielding because the crystalline phase becomes loose and flexible with increasing T_E (Fig. 5(a)). On the contrary, lamellar disintegration should occur at increasing strains, which demands $U_{CEAM}(\varepsilon_y)$ to increase correspondingly until $\sigma_{CEAM}(\varepsilon_y)$ reaches its critical value.

4.3. Deformation of the CEAM network

The deformation of the CEAM network is only related to the parameter M_{PT} in Eq. (5c). The fitted value of M_{PT} is plotted against T_E in Fig. 8(a). M_{PT} decreases with T_E at temperatures below 400 K, above which M_{PT} becomes close

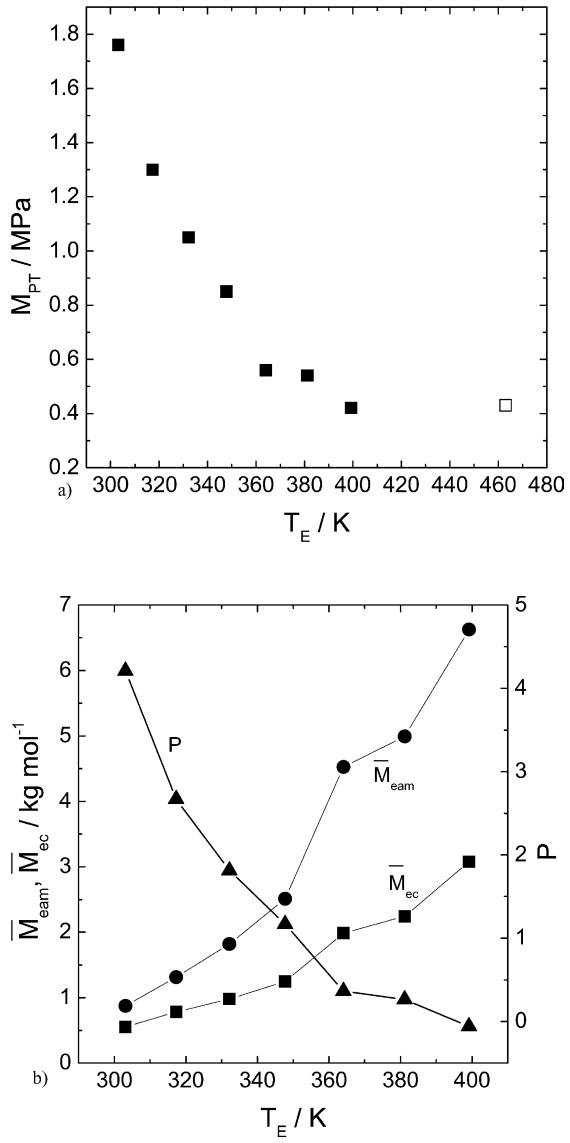

Fig. 8. (a) T_E dependence of apparent shear modulus M_{PT} for the CEAM-network, and (b) T_E dependences of the molecular weights $\bar{M}_{ec}$ and $\bar{M}_{eam}$ as well as the numbers P of the crystalline and the amorphous sequences. The point with open symbol in (a) is a reference value of the plateau modulus $G_N^0 = 0.43$ MPa in the melt [23]. The solid curves in (b) are for guidance of eye.

to the plateau modulus $G_N^0 = 0.43$ MPa in the melt [23]. This dependence of M_{PT} on T_E is of course in contradiction with the classical rubber elasticity theory. However, it is not unexpected taking the temperature dependence of the crystallinity and crystal size into consideration.

Crystallization of polymers from the quiescent melt does not lead to a resolution of the existing entanglements but just shift them into the amorphous regions [24]. Strobl and coworkers found that, at room temperature, the network shear modulus of polyethylene and related copolymers increase with increasing crystallinity, essentially starting at the value of the melt. Crystallites in semicrystalline state act as crosslinks and fillers [25]. In this work, the linear relationship between M_{PT} and V_c does not hold because of the variations in structure, size and density of crystallites with T_E.

Taking the crosslinking and the filler effects of crystallites into consideration, the shear modulus may be expressed [26–29] as

$$M_{PT} = \nu k T_E (1 - V_C)(1 + 2.5V_c) \quad (6)$$

where k is Boltzmann constant and ν is the density of elastically effective network strands in the amorphous phase.

For simplicity, let us assume that a strand of $\bar{M}_e = 6900$ g mol^{-1} in the melt [23] forms crystalline sequences of $a\bar{M}_{ec}$ in molecular weight broken up alternatively by amorphous sequences of $\bar{M}_{eam}$ in molecular weight in the semicrystalline state. The crystalline sequences should be apart away from the entanglement points and therefore introduction of P crystalline sequences leads to $(P+1)$ amorphous sequences in the previous entanglement strand, thus

$$\nu = \nu_0(P + 1) \quad (7)$$

In the melt with $V_c = 0$ and $P = 0$, Eq. (6) is reduced to $M_{PT} = \nu_0 k T_E$. The molecular weights $\bar{M}_{ec}$ and $\bar{M}_{eam}$of the crystalline and the amorphous sequences are related to the sequence number P by

$$\bar{M}_e = (P + 1)\bar{M}_{eam} + P\bar{M}_{ec} \quad (8a)$$

$$a\frac{\bar{M}_e}{\rho}V_c = P\frac{\bar{M}_{ec}}{\rho_c} \quad (8b)$$

In Eqs. (8a) and (8b), density ρ can be evaluated from those of the crystalline and the amorphous phases, ρ_c and ρ_{am}, as $\rho = \rho_c V_c + \rho_{am}(1 - V_c)$, and ρ_c and ρ_{am} can be estimated using the relations of Danusso et al [30].

Substituting values of M_{PT} and V_c into Eq. (6), we can estimate P, and then obtain $\bar{M}_{eam}$ and $\bar{M}_{ec}$ by solving Eqs. (8a) and (8b). Results are plotted in Fig. 8(b) as a function of T_E. It is seen that both $\bar{M}_{eam}$ and $a\bar{M}_{ec}$ increase with T_E below 400 K, which are related to the melting of tiny crystallites and the resultant lamellar thickening. The Bragg spacing L_0 of a quenched iPP sample by Wang [18] et al. was used to calculate the average lamellar thickness L_c and the average thickness of amorphous layer L_{am} according to the two-phase model applying V_c measured in this work, i.e., $L_c = L_0 V_c$ and $L_{am} = L_0(1 - V_c)$ [31]. The result in Fig. 9 shows that both L_c and L_{am} increases with increasing temperature below 400 K, which is roughly consistent with the variations of $\bar{M}_{ec}$ and $\bar{M}_{eam}$.

Semicrystalline polymers usually exhibit a broad melting range due to the wide distribution of the lamellar thickness. The melting temperature of a given lamella increases with its thickness [32]. It is plausible that quenching of the iPP film produces a lot of tiny crystallites with various sizes in the entanglement network of melt. When the quenched sample is heated, the less stable thin lamellae in the smectic form melt first and then recrystallize into the α-form at greater thicknesses, which leads the average lamellar thickness to increase with temperature before complete melting. Amorphous chains may also recrystallize onto survival lamellae via diffusion [33]. The endotherm and exotherm below 400 K in DSC curve (Fig. 2) are attributed to melting of tiny crystallites followed by growth of crystallites in size or thickness. Result in Fig. 8(b) indicates that the decrease in M_{PT} with T_E below 400 K is mainly due to the decrease in crystal number and the increase in molecular weight of elastically effective segments.

4.4. Solid deformation at temperatures close to T_m

The yielding at $T_E > 400$ K in Fig. 1(a) is still related to breakdown of remaining crystals. However, local melting agitated by strain energy might be the most significant effect invoking several necks to appear in the film. These necks with different deformation levels move back and forth along

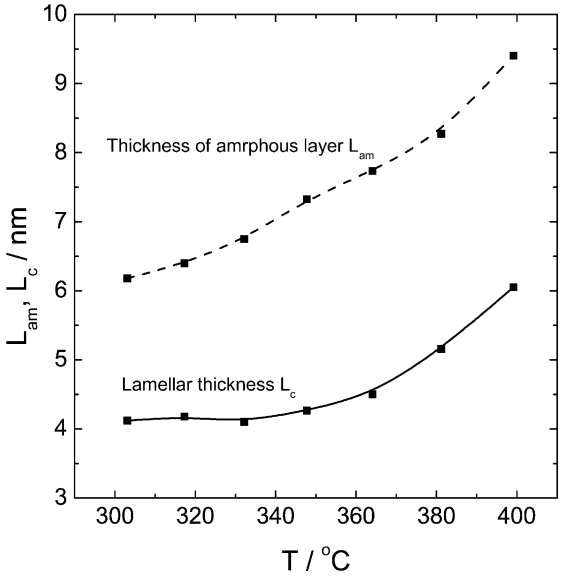

Fig. 9. (a) Thicknesses of lamella and amorphous layer calculated from Bragg spacing of a quenched iPP sample by Wang et al. [18] and the crystallinity measured in this work.

the draw axis, leading to the wavy f_{av} profile in Fig. 1(b). The local melting may induce molecular relaxation in the amorphous phase accompanying the overall orientation increment. On the other hand, the strain-induced recrystallization from oriented amorphous chain leads to the increases in K' and K as compared with their constant values at lower T_Es in Fig. 3.

The local melting prevents the amorphous chain from affine deformation and the IPN model is thereby not applicable at T_Es located at the main melting region. After a fraction of crystallites melts away, the crystalline phase cannot preserve certain continuity necessary for forming the C network spreading through the whole sample, i.e., the crystalline phase becomes discontinuous. Accordingly, the CEAM network is reduced to the entanglement network in which trapped entanglements might undergo relaxation motion at long times or high strains, which accounts for the measured σ lower than the predicted one as shown in Fig. 4. Furthermore, when the film is stretched at a constant elongation rate up to a pretty large strain, the corresponding strain rate must decrease continuously so as to give smaller and smaller viscous force. This also partially explains why the IPN model becomes inapplicable at large λ_{Meso}.

5. Conclusion

Linear relationship between f_c and f_{av} holds for $f_{av} \leq 0.5$ for the deformation of quenched iPP film over a broad T_E range from room temperature to the melting point. The slopes of the linear portion between f_c and f_{av} as well as between f_c and f_{am} are independent of T_E at $303\ K \leq T_E \leq 399\ K$, whereas they increase abruptly at higher T_Es where the main melting occurs significantly as revealed from the DSC measurement. The IPN model can fairly describe the mesoscale deformation during the localized necking at $303\ K \leq T_E \leq 399\ K$ but is invalid for higher T_Es.

By applying the IPN model to deformation at $303\ K \leq T_E \leq 399\ K$, it is found that $E(C)$ and $\sigma_y(C)$ as a function of T_E obey the Arrhenius law, which suggests that changes in intermolecular interaction dominate the activation process in the C network. The C network yields at almost constant total yield energy and also constant stress of $\sigma_{CEAM}(\varepsilon_y)$, the later being the critical value exerted by the CEAM network necessary for chains to be pulled out from lamellar fragments. M_{PT} of the CEAM network as a function of T_E is explained in relation to V_c, and the variations of molecular weights and the numbers of crystalline and the amorphous sequences between two successive entanglements. Increasing T_E results in a reduction in the number of crystalline blocks along a chain strand but leads to considerable lamellar thickening.

Acknowledgements

This work has been partially supported by the Grant-in-Aid for the Scientific Research from Ministry of Education, Culture, Sports, Science and Technology, Japan (No. 10305070) and one of the authors, Y. Song, is grateful to JSPS for the Grant-in-Aid for JSPS Fellows relating to JSPS Fellowship for Foreign Researchers (No. 12000317) during his stay in Japan for a postdoctoral research.

References

[1] Shigematsu Y, Takada A, Nemoto N, Nitta K. Rev Sci Instrum 2001; 72:3927.
[2] Song Y, Shigematsu Y, Nitta K-H, Nemoto N. Polym J 2002;34:584.
[3] Song Y, Nitta K-H, Nemoto N. Macromolecules 2003;36:1955.
[4] Song Y, Nitta K-H, Nemoto N. Macromolecules 2003;36:8066.
[5] Vadimsky RG, Keith HD, Padden FJ. J Polym Sci 1969;7:1367.
[6] Takayanagi M, Nitta K-H. Macromol Theory Simul 1997;6:181.
[7] Song Y, Yamamoto H, Nemoto N. Macromolecules 2004;37: 6219.Song Y, Nemoto N. J Polym Sci Part B: Polym Phys, accepted. Naka Y, Nemoto N, Song Y. J Polym Sci Part B: Polym Phys, 2005;43;1520.
[8] Capaccio G, Ward IM. Nat Phys Sci 1973;243:143. Capaccio G, Ward IM. Polymer 1975;16:239. Capaccio G, Crompton TA, Ward IM. J Polym Sci, Polym Phys Ed 1976;14:1641.
[9] Capaccio G, Ward IM. Colloid Polym Sci 1982;260:46.
[10] Sadler DM, Barham PJ. Polymer 1990;31:36. Sadler DM, Barham PJ. Polymer 1990;31:43.
[11] Snyder RG, Schachtschneider JH. Spectro Acta 1964;20:853.
[12] Siesler HW. Adv Polym Sci 1984;65:1.
[13] Samuels R. J Makromol Chem Suppl 1981;4:241.
[14] Kong Y, Hay JN. Polymer 2002;43:3873. Kong Y, Hay JN. Eur Polym J 2003;39:1721.
[15] Saraf RF, Porter RS. J Polym Eng Sci 1988;28:842.
[16] Saraf RF, Porter RS. J Rheol 1987;31:59.
[17] Seguela R, Staniek E, Escaig E, Fillon E. J Appl Polym Sci 1999;71: 1873.
[18] Wang Z, Hsiao BS, Srinivas S, Brown GM, Tsou AH, Cheng SZD, et al. Polymer 2001;42:7561.
[19] Androsch R, Wunderlich B. Macromolecules 2001;34:5950.
[20] Saraf RF, Porter RS. J Polym Eng Sci 1988;28:842.
[21] Darras O, Séguéla R. J Polym Sci, Part B: Polym Phys 1993;31:759.
[22] Nitta K-H, Takayanagi M. J Polym Sci, Part B: Polym Phys 2000;38: 1037.
[23] Fetters LJ, Lohse DJ, Garacia-Franco CA, Brant P, Richter D. Macromolecules 2002;35:10096.
[24] Strobl G. The physics of polymers. New York: Springer; 1997.
[25] Hiss R, Hobeika S, Lynn C, Strobl G. Macromolecules 1999;32:4390. Al-Hussein M, Strobl G. Macromolecules 2002;35:8515.
[26] Treloar RLG. The physics of rubber elasticity. 3rd ed. Oxford: Clarendon Press; 1975.
[27] Ryu CY, Ruokolainen J, Fredrickson GH, Kramer EJ, Hahn SF. Macromolecules 2002;35:2157.
[28] Smallwood HM. J Appl Phys 1944;15:758.
[29] Guth E. J Appl Phys 1945;16:20.
[30] Danusso F, Moraglio G, Ghiglia W, Motta L, Talamini G. Chim Ind 1959;41:748.
[31] Ryan AJ, Stanford JL, Bras W, Nye TMW. Polymer 1997;38:759.
[32] Wunderlich B. Macromolecular physics. New York: Academic Press; 1980.
[33] Scott DC, Daxaben P. Polymer 1994;35:1855.